



Synthesis, characterization, and photocatalytic activity of sol–gel prepared Mg/ZnO nanoparticles

Nahide Zarei, Mohammad A. Behnajady*

Department of Chemistry, Tabriz Branch, Islamic Azad University, Tabriz, Iran, Tel. +98 09144187973; email: n.zarei745@gmail.com (N. Zarei), Tel. +98 41 33396136; Fax: +98 41 33333458; emails: behnajady@gmail.com, behnajady@iaut.ac.ir (M.A. Behnajady)

Received 26 September 2014; Accepted 12 August 2015

ABSTRACT

In this study, ZnO nanoparticles with different Mg contents and calcination temperatures were synthesized by the sol–gel method. The photocatalytic activity of the synthesized nanoparticles was investigated in the photocatalytic degradation of Rhodamine B. The products were characterized by X-ray diffraction (XRD), energy dispersive X-ray spectroscopy (EDX)-mapping, scanning electron microscopy (SEM), transmission electron microscopy (TEM), diffuse reflectance spectroscopy (DRS), and Brunauer–Emmett–Teller (BET) techniques. The XRD results showed that the doped nanoparticles had the same crystal structure as the pure ZnO. The EDX and mapping findings indicated the existence of Mg in the doped sample. SEM and TEM analysis showed the spherical shape and uniform-size distribution of the nanoparticles. Based on DRS spectra, the band gap energy value of 2.0 wt% Mg doped ZnO was 3.26 eV, which was larger than the ZnO nanoparticles' band gap energy. Using BET analysis, the surface areas of ZnO and 2.0 wt% Mg/ZnO were calculated to be 14.9 and 22.5 m² g⁻¹, respectively. The results of the photocatalytic activity indicated that Mg/ZnO was more active than pure ZnO photocatalyst due to its higher surface area and larger band gap energy. Maximum photocatalytic activity was achieved for Mg/ZnO nanoparticles with 2.0 wt% Mg and at the calcination temperature of 400°C.

Keywords: Heterogeneous photocatalysis; Mg/ZnO nanoparticles; Rhodamine B; Sol–gel

1. Introduction

Wastewater from textile, paper, and some other industries contain residual dyes, which are not readily biodegradable [1]. Due to its complex bio-resistant content, various physical, chemical, and biological technologies should be utilized for treating this type of wastewater. Advanced oxidation processes (AOPs) use catalysts or oxidant compounds concomitant with ultraviolet (UV) or visible light, which generate highly

reactive transient species such as hydroxyl radicals with a high potential for oxidation of organic compounds. Among various AOPs, the heterogeneous photocatalysis processes are very promising techniques compared with the traditional processes. Heterogeneous photocatalysis is based on the absorption of photons by a semiconductor with appropriate band gap energy. The semiconductor photocatalyst should be chemically and biologically inert, stable, inexpensive, and without any human and environmental risks [2]. When the semiconductor photocatalyst is illuminated

*Corresponding author.

by UV light, the electrons are promoted from valence band (VB) to the conduction band (CB) to generate photo-induced electron–hole pairs [3–5]. The holes can oxidize water or hydroxide ions to produce hydroxyl radicals [6–8]. The results of electron paramagnetic resonance (EPR) indicate that the electrons and holes are trapped in different defect sites [9]. The dissolved oxygen reduces with photo-induced electrons, which is another source of hydroxyl radicals [10].

Zinc oxide (ZnO) nanoparticles have been the focus of intense interest due to their potential wide range applications in electronics, optics, optoelectronics, and lasers. The photosensitive properties of ZnO nanoparticles make it a good candidate for photocatalytic application in the degradation of various pollutants. However, the recombination of photo-induced electron–hole pairs leads to low photocatalytic activity [11]. The modification of the semiconductors with noble metals has attracted significant attention, especially to heterogeneous photocatalysis [12]. Recently, some metal ions such as Ag^+ , Cd^{2+} , Fe^{2+} , Mn^{2+} , and Co^{2+} have been used as doping ions to reduce the recombination of electron–hole pairs. Mg^{2+} could be a proper metal ion in doping ZnO nanoparticles due to its similar ionic radius to Zn, low cost, and non-toxicity [11]. The highest photocatalytic activity of Mg-doped TiO_2 , in comparison with other M-doped TiO_2 catalysts (M = Fe, Co, Ce, Cr, Mn, Ni, and Ag ions), was reported by Feng et al. [13] for the degradation of RhB in aqueous solution. Behnajady et al. [14] observed a superior photocatalytic activity for Mg-doped TiO_2 compared to bare TiO_2 for the degradation of C.I. Acid Red 27. Abdollahi et al. [15] synthesized ZnO nanoparticles' doped manganese via precipitation method. The results of their study revealed a better photocatalytic activity for 2.0 wt% Mn doped ZnO in the removal of cresol. Fu et al. [16] prepared Cu-doped ZnO nanoparticles using sol–gel method. Photocatalytic activity was tested in the degradation of Methyl Orange (MO). Degradation rate of MO in the presence of 0.5% Cu/ZnO nanoparticles was achieved 88.0%, which exceeded that of undoped ZnO. Lu et al. [11] also synthesized Mg-doped ZnO nanoparticles by sonochemical method, reporting that Mg-doped ZnO nanoparticles presented better properties in photocatalytic degradation of Methylene Blue (MB) than pure ZnO nanoparticles. Oh et al. [17] prepared the Mg/ZnO nanoparticles through a facile one-step sonochemical method. The examination of their optical properties showed a blue shift of the band gap through Mg doping. In another study, Kant and Kumar [18] investigated the removal of MB under UV–vis region in the presence of ZnO and Ni-doped ZnO nanospheres. The degradation rate of MB in the

presence of the synthesized samples improved in comparison to the undoped ZnO under visible light irradiation. Etacheri et al. [19] also prepared Mg-doped ZnO nanoparticles by an oxalate co-precipitation method. The photocatalytic activity of the synthesized nanoparticles in the removal of MB was investigated under irradiation of Q-Sun solar simulator as the light source. The most active sample was 0.1% Mg/ZnO calcined at 600°C, which indicated a twofold enhancement in the sun light-induced photocatalytic decomposition of the methylene blue.

In the present study, the synthesis of ZnO and Mg-doped ZnO nanoparticles was carried out by the sol–gel method, and the effect of Mg doping content and calcination temperature on the photocatalytic activity in the removal of RhB, as a model pollutant from an aqueous solution, was investigated.

2. Materials and methods

2.1. Materials

Zinc acetate di-hydrate, oxalic acid, and ethanol were obtained from Merck, and magnesium nitrate was purchased from Scharlau. RhB (Merck) is a dye belonging to a class of compounds called xanthenes. Its chemical structure and other characteristics are listed in Table 1.

2.2. Preparation of ZnO nanopowders

In a typical experiment, the zinc acetate dihydrate (2.19 g) was dissolved in ethanol (100 mL) at 60°C and stirred for 30 min. The oxalic acid (2.51 g), dissolved in ethanol (40 mL) at 60°C, was slowly added to the warm ethanolic solution of zinc acetate. The mixture was stirred for 2 h. Then, it was dried at 80°C for 12 h. The dried xerogel was further calcined at 400°C for 2 h to form ZnO nanopowder [12].

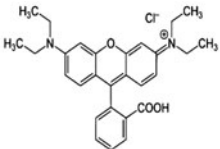
2.3. Preparation of Mg-doped ZnO nanopowders

To synthesize Mg-doped ZnO, various weights % (0.2, 0.5, 1, 1.5, 2, and 3) of the magnesium nitrate dissolved in ethanol (20 mL) were added to the zinc acetate-oxalic acid solution while the solution was being stirred. This solution was dried as above and calcined at different temperatures (400–800°C) for 2 h.

2.4. The measurement of photocatalytic activity

All of the experiments were carried out at ambient temperature in a batch quartz reactor. The irradiation

Table 1
Characteristics of RhB

Structure	Molecular formula	λ_{\max} (nm)	M_w (g mol ⁻¹)	Appearance
	C ₂₈ H ₃₁ ClN ₂ O ₃	554	479.02	Red to violet powder

source was provided by UV-C lamp (15 W, Philips Co. $\lambda_{\max} = 254$ nm), which was positioned parallel to the light source. For the photocatalytic degradation of RhB, 40 mg of catalyst was dispersed in 100 mL of distilled water for 15 min, using an ultrasonic bath (Elma T460/H, 35 kHz, 170 W); then the desired concentration of RhB (10 mg L⁻¹) and photocatalyst suspension (ZnO or Mg/ZnO) were transferred into the quartz tube reactor and stirred for 15 min in the dark and in the presence of oxygen to establish the surface adsorption equilibrium. With turning on the UV lamp, the photocatalytic reaction was initiated. At definite time intervals (3 min), the samples (5 mL) were taken out and centrifuged (Hettich EBA 8S). Then, the concentration of RhB was analyzed by UV-vis spectrophotometer (Pharmacia Biotech Ultraspec 2000) at $\lambda_{\max} = 554$ nm.

2.5. Characterization methods

The crystallite size and crystalline phase of the synthesized nanoparticles were analyzed using X-ray diffraction (XRD) (Siemens D5000 diffractometer). The surface morphology and particle size of the photocatalyst were analyzed by transmission electron microscopy (TEM) (Philips CM10). The morphology was characterized by scanning electron microscopy (SEM) with an energy dispersive X-ray (EDX) and mapping (Tescan MIRA3FEG). The diffuse reflectance spectroscopy (DRS) spectra of samples were recorded using an Avaspec 2048 TEC spectrophotometer. The specific surface area (BET) of the samples was obtained by the Belsorp mini II.

3. Results and discussion

3.1. Characterization of the prepared nanoparticles

In order to investigate the changes in the crystal structure, XRD measurements were carried out in the range of 2θ diffraction angles between 20° and 75° for ZnO and Mg/ZnO nanoparticles. The diffraction

patterns of ZnO and Mg-doped ZnO nanoparticles calcined at 400°C are shown in Fig. 1. As shown in the figure, the XRD patterns indicate that only the peaks

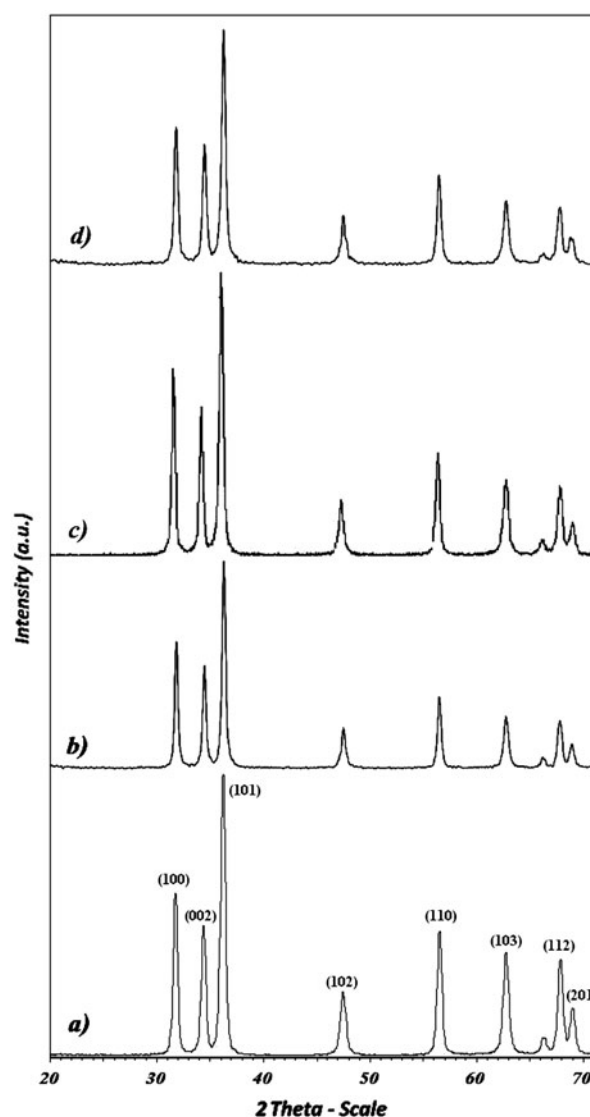


Fig. 1. XRD patterns of (a) ZnO, (b) Mg 1.0%/ZnO, (c) Mg 2.0%/ZnO, and (d) Mg 3.0%/ZnO calcined at 400°C.

correspond to the ZnO, and there is no sign of Mg peaks due to its low content. The crystallite sizes (D) were estimated by using Scherrer equation (Eq. (1)):

$$D = \frac{k\lambda}{\beta \cos \theta} \quad (1)$$

where D is the diameter of the crystallite size, k is the constant value of 0.89, λ is the wavelength (Cu $k\alpha$), θ is diffraction angle, and β is the half-width of the diffraction peak [20]. The results showed that the crystallite sizes of Mg-doped ZnO nanoparticles were more than those of the pure ZnO nanoparticles. The crystallite sizes of ZnO and Mg/ZnO nanoparticles containing 1, 2, and 3% Mg were calculated to be 18, 20, 23, and 20 nm, respectively.

Fig. 2 shows the TEM image of 2.0 wt% Mg/ZnO nanoparticles. As it is evident in Fig. 2, the synthesized nanoparticles have agglomerated to larger particles. The SEM image of the 2.0 wt% Mg/ZnO nanoparticles in Fig. 3 shows their spherical shape and uniform-size distribution. The EDX spectrum in Fig. 4 gives the chemical composition of the materials at the microscopic level and shows that the 2.0 wt% Mg/ZnO consists of Mg, Zn, and O elements. The mapping images of Zn and Mg are shown in Fig. 5, which proves uniform distribution of Mg and Zn.

The specific surface area (BET), volume, and average diameter (BJH) of the catalysts were determined by N_2 adsorption at 77 K. Fig. 6 displays the N_2 adsorption–desorption isotherms of pure ZnO and 2.0 wt% Mg/ZnO nanoparticles. The results (Fig. 6), according

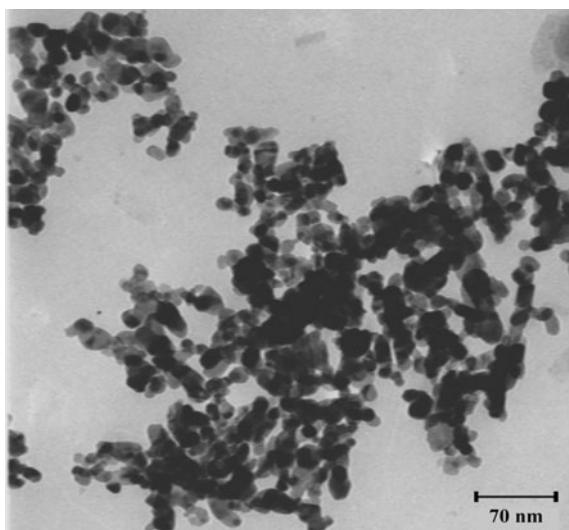


Fig. 2. TEM micrograph of Mg 2.0%/ZnO calcined at 400°C.

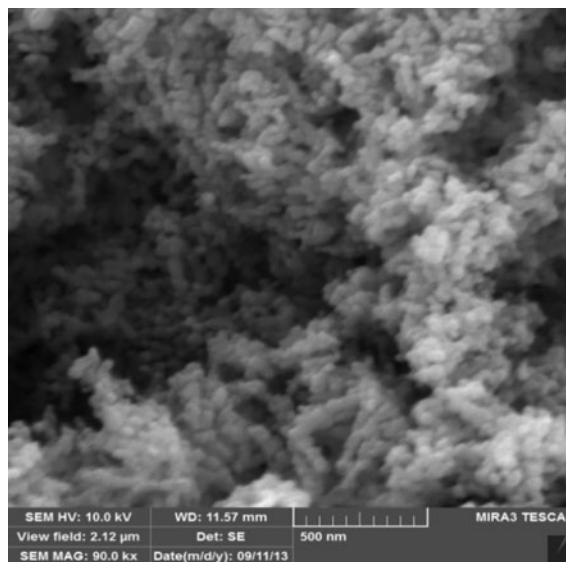


Fig. 3. SEM micrograph of Mg 2.0%/ZnO calcined at 400°C.

to IUPAC classification, display a Type-III isotherm, indicating that nanoparticles contained both mesoporous and macroporous materials. The specific surface areas of ZnO and Mg/ZnO nanoparticles were obtained to be 14.9 and 22.5 $m^2 g^{-1}$, respectively. Table 2 summarizes the total pore volume and means pore diameter of ZnO and 2.0 wt% Mg/ZnO nanoparticles.

Fig. 7 shows the diffuse reflectance spectra of ZnO and Mg/ZnO nanoparticles. The calculated band gap energies were 3.21 and 3.26 eV for ZnO and Mg/ZnO, respectively. The results indicated that doping with Mg led to the increase of the band gap energy by 0.05 eV, indicating a blue shift.

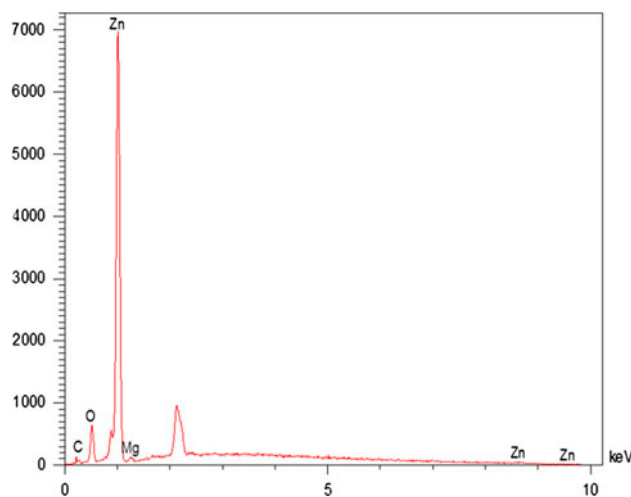


Fig. 4. EDX spectra of Mg 2.0%/ZnO calcined at 400°C.

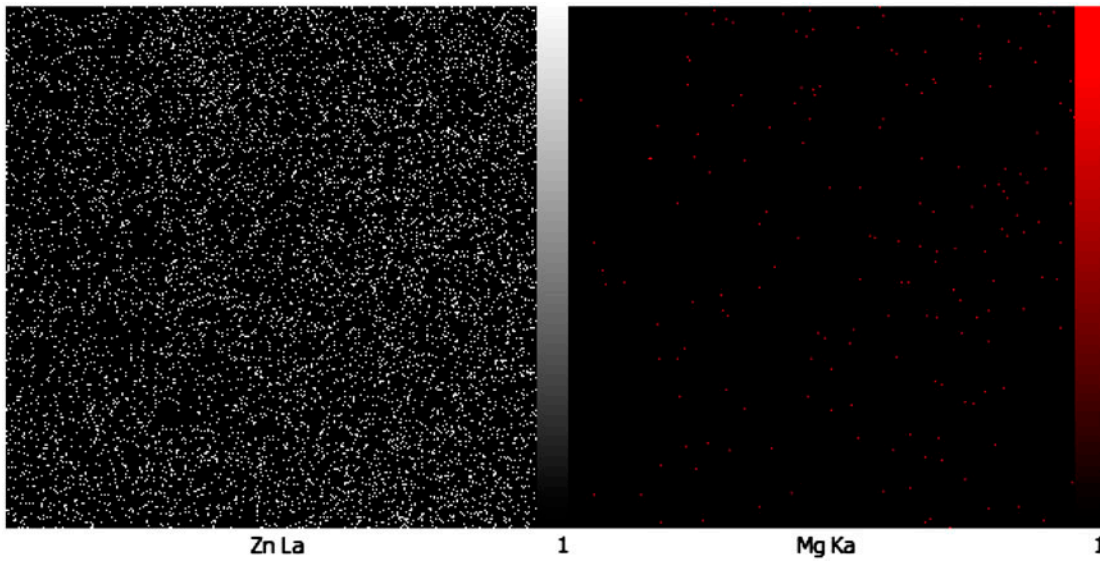


Fig. 5. Mapping of (a) Zn and (b) Mg for Mg 2.0%/ZnO calcined at 400°C.

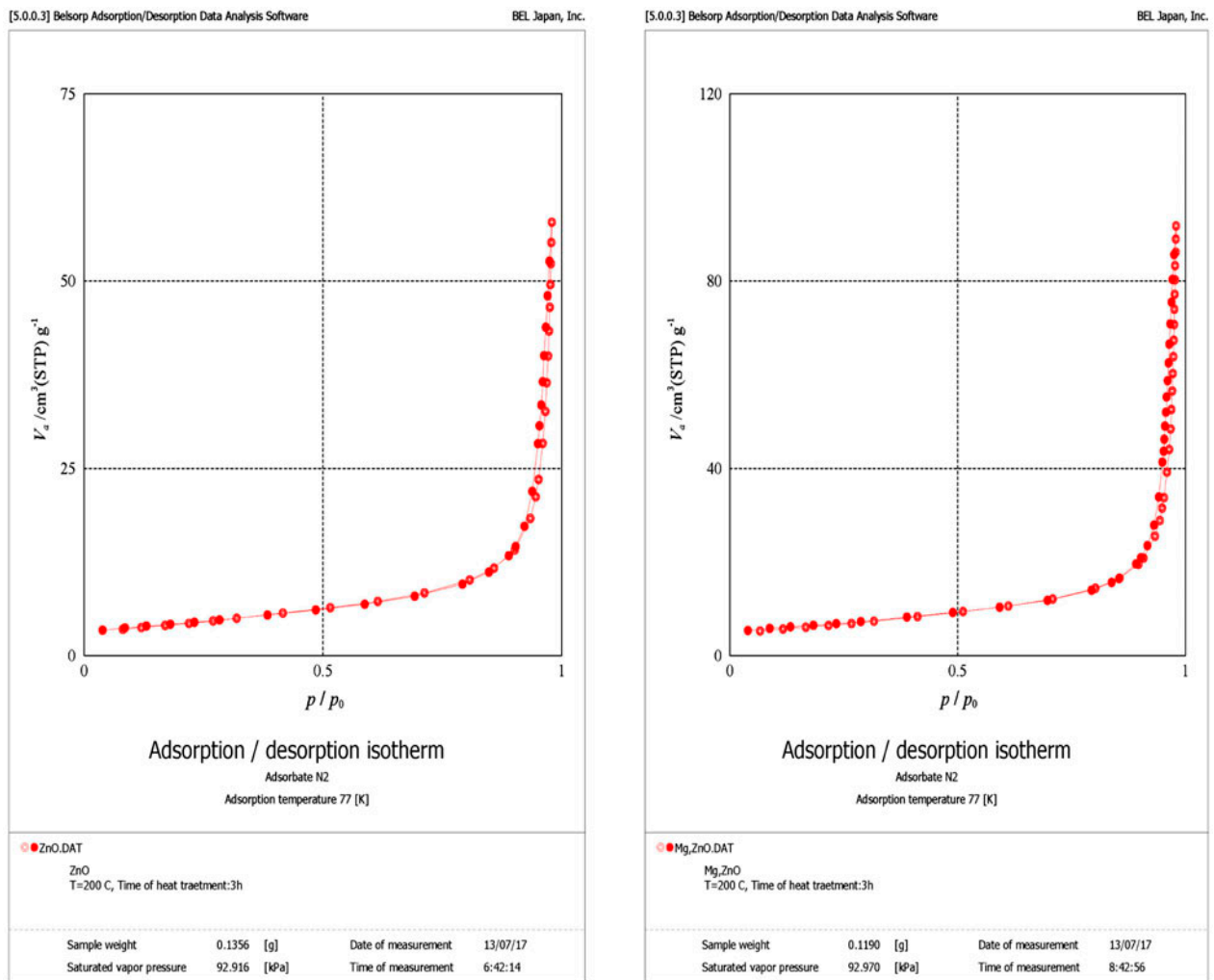


Fig. 6. Adsorption–desorption isotherm of ZnO and Mg 2.0%/ZnO calcined at 400°C.

Table 2

Pore characterization of ZnO and 2.0 wt% Mg/ZnO calcined at 400°C

Catalyst	Total pore volume (cm ³ g ⁻¹)	Mean pore diameter (nm)
ZnO	0.089486	24.038
Mg/ZnO	0.1419	25.461

3.2. Photocatalytic activity results

The evaluation of the treatment costs is one of the aspects which need greater attention. Since the UV/ZnO process is electric-energy-intensive, simple figures-of-merit based on electric energy consumption can be very useful and informative. Bolton et al. [21] defined the figures-of-merit “electric energy per order” (E_{EO}) for using in AOPs. In the case of low pollutant concentrations (which applies here), the appropriate figure-of-merit is the electrical energy per order (E_{EO}), defined as the number of kilowatt hours of electrical energy required to reduce the concentration of a pollutant by one order of magnitude in a unit volume of contaminated water. The E_{EO} (kW h/m³/order) can be calculated using the following equation for a batch type reactor:

$$E_{EO} = \frac{P_{el} \times t \times 1000}{V \times 60 \times \log(C_0/C)} \quad (2)$$

where P_{el} is the input power (kW) to the AOP system, t is the irradiation time (min), V is the volume of water (L) in the reactor, and C_0 and C are the initial and final pollutant concentrations, respectively.

3.2.1. The effect of Mg content

The effect of Mg doping in ZnO lattice on E_{EO} values is shown in Table 3. According to the results, the E_{EO} value decreased with increasing Mg amount up to

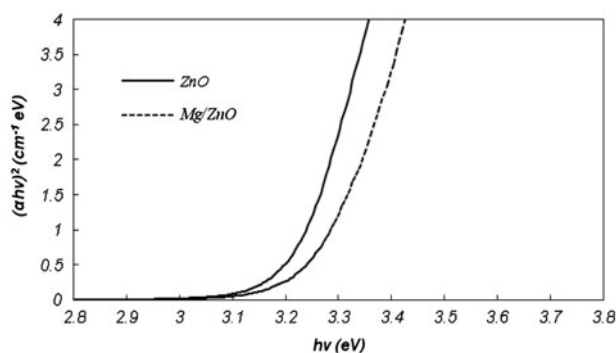


Fig. 7. The DRS spectra of ZnO and Mg 2.0%/ZnO calcined at 400°C.

Table 3

E_{EO} values for removal of RhB in the various Mg percent and calcination temperature

Mg (%)	Calcination temperature	E_{EO} (kW h/m ³ /order)
0	400	115.57
0.2	400	86.00
0.5	400	63.34
1	400	58.40
1.5	400	52.12
2	400	37.32
3	400	44.12
2	500	62.14
2	600	65.59
2	700	120.35
2	800	223.50

2.0%. Increasing the Mg content to 3% raised the E_{EO} value. It is clear that the photocatalytic activity of semiconductors is proportionate to their band gap energy. The higher band gap energy corresponds to stronger electron–hole pairs causing higher photocatalytic activity. Thus, the larger band gap of Mg/ZnO nanoparticles, according to the DRS results, leads to higher photocatalytic activity and consequently lower E_{EO} value. Moreover, increasing the photocatalytic activity by increasing Mg content up to the optimized value could be attributed to crystal deficiency. Doping with Mg causes lattice deficiency, eventually inducing crystal deficiency. The deficiency inhibits the recombination of electron–hole formation, so the photocatalytic activities improve proportionally. However, if the dopant is increased above the optimized value, the various effects decrease photocatalytic activity because of the decrease in specific surface areas and inhibition of reagents surface adsorption [22].

3.2.2. The effect of calcination temperature

The results in Table 3 demonstrate the effect of calcination temperature on Mg/ZnO photocatalytic activity. They indicate the minimum E_{EO} value for Mg/ZnO photocatalyst doped by 2.0 wt% of Mg and calcination temperature of 400°C. Increasing E_{EO} value or decreasing photocatalytic activity by increasing calcination temperature could be attributed to the increase in crystallite size of particles, agglomeration of nanoparticles, and reduction of adsorbed H₂O on catalyst surface [23].

4. Conclusion

To increase the photocatalytic activity of ZnO nanoparticles and decrease the electrical energy consumption in this process, Mg/ZnO nanoparticles were

synthesized by the sol–gel method. In order to evaluate the photocatalytic activity of the synthesized photocatalyst, RhB photodegradation was studied under UV-C irradiation. The results indicated that the optimized values of Mg content and calcination temperature were 2.0 wt% and 400 °C, respectively. The synthesized nanoparticles were characterized by XRD, SEM, EDX-Mapping, TEM, DRS, and Brunauer–Emmett–Teller (BET) techniques. The XRD results indicated that ZnO and Mg/ZnO had the same crystallite structure. The SEM and TEM images showed uniform size distribution and spherical particles for Mg/ZnO nanoparticles. The BET analysis showed that the surface area of Mg/ZnO nanoparticles was higher than that of ZnO nanoparticles. From DRS spectra, the band gap energies for ZnO and Mg/ZnO were calculated to be 3.21 and 3.26 eV. The results also revealed that doping ZnO nanoparticles with Mg under an optimized concentration of Mg and calcination temperature was an adequate method to intensify its photocatalytic activity.

Acknowledgments

The authors would like to thank the financial support of Tabriz Branch, Islamic Azad University and the Iranian Nanotechnology Initiative Council.

References

- [1] M.A. Behnajady, N. Modirshahla, R. Hamzavi, Kinetic study on photocatalytic degradation of C.I. Acid Yellow 23 by ZnO photocatalyst, *J. Hazard. Mater.* 133 (2006) 226–232.
- [2] M.C. Cotto-Maldonado, T. Campo, E. Elizalde, A. Gomez-Martinez, C. Morant, F. Marquez, Photocatalytic degradation of Rhodamine-B Under UV-visible light irradiation using different nanostructured catalysts, *Am. Chem. Sci. J.* 3 (2013) 178–202.
- [3] M.A. Behnajady, N. Modirshahla, Nonlinear regression analysis of kinetics of the photocatalytic decolorization of an azo dye in aqueous TiO₂ slurry, *Photochem. Photobiol. Sci.* 5 (2006) 1078–1081.
- [4] M.A. Behnajady, N. Modirshahla, N. Daneshvar, M. Rabbani, Photocatalytic degradation of C.I. Acid Red 27 by immobilized ZnO on glass plates in continuous-mode, *J. Hazard. Mater.* 140 (2007) 257–263.
- [5] M.A. Rauf, S. Ashraf, Fundamental principles and application of heterogeneous photocatalytic degradation of dyes in solution, *Chem. Eng. J.* 151 (2009) 10–18.
- [6] H.D. Mansilla, C. Bravo, R. Ferreyra, M.I. Litter, W.F. Jardim, C. Lizama, J. Freer, J. Fernández, Photocatalytic EDTA degradation on suspended and immobilized TiO₂, *J. Photochem. Photobiol. A: Chem.* 181 (2006) 188–194.
- [7] C.H. Wu, C.L. Chang, C.Y. Kuo, Decolorization of Procion Red MX-5B in electrocoagulation (EC), UV/TiO₂ and ozone-related systems, *Dyes Pigm.* 76 (2008) 187–194.
- [8] M.A. Behnajady, N. Modirshahla, N. Daneshvar, M. Rabbani, Photocatalytic degradation of an azo dye in a tubular continuous-flow photoreactor with immobilized TiO₂ on glass plates, *Chem. Eng. J.* 127 (2007) 167–176.
- [9] X. Chen, S.S. Mao, Titanium dioxide nanomaterials: Synthesis, properties, modifications, and applications, *Chem. Rev.* 107 (2007) 2891–2959.
- [10] Z. Wang, C. Chen, F. Wu, B. Zou, M. Zhao, J. Wang, C. Feng, Photodegradation of Rhodamine B under visible light by bimetal codoped TiO₂ nanocrystals, *J. Hazard. Mater.* 164 (2009) 615–620.
- [11] X. Lu, Z. Liu, Y. Zhu, L. Jiang, Sonochemical synthesis and photocatalytic property of zinc oxide nanoparticles doped with magnesium(II), *Mater. Res. Bull.* 46 (2011) 1638–1641.
- [12] R. Georgekutty, M.K. Seery, S.C. Pillai, A highly efficient Ag–ZnO photocatalyst: Synthesis, properties, and mechanism, *J. Phys. Chem. C* 112 (2008) 13563–13570.
- [13] H. Feng, L.E. Yu, M.H. Zhang, Ultrasonic synthesis and photocatalytic performance of metal-ions doped TiO₂ catalysts under solar light irradiation, *Mater. Res. Bull.* 48 (2013) 672–681.
- [14] M.A. Behnajady, B. Alizade, N. Modirshahla, Synthesis of Mg-doped TiO₂ nanoparticles under different conditions and its photocatalytic activity, *Photochem. Photobiol.* 87 (2011) 1308–1314.
- [15] Y. Abdollahi, A.H. Abdullah, Z. Zainal, N.A. Yusof, Synthesis and characterization of manganese doped ZnO nanoparticles, *Int. J. Basic Appl. Sci.* 11 (2011) 62–69.
- [16] M. Fu, Y. Li, S. Wu, P. Lu, J. Liu, F. Dong, Sol–gel preparation and enhanced photocatalytic performance of Cu-doped ZnO nanoparticles, *Appl. Surf. Sci.* 258 (2011) 1587–1591.
- [17] J.Y. Oh, S.C. Lim, S.D. Ahn, S.S. Lee, K.I. Cho, J.B. Koo, R. Choi, M. Hasan, Facile one-step synthesis of magnesium-doped ZnO nanoparticles: Optical properties and their device applications, *J. Phys. D: Appl. Phys.* 46 (2013) 285101.
- [18] S. Kant, A. Kumar, A comparative analysis of structural, optical and photocatalytic properties of ZnO and Ni doped ZnO nanospheres prepared by sol–gel method, *Adv. Mater. Lett.* 3 (2012) 350–354.
- [19] V. Etacheri, R. Roshan, V. Kumar, Mg-doped ZnO nanoparticles for efficient sunlight-driven photocatalysis, *ACS Appl. Mater. Interfaces* 4 (2012) 2717–2725.
- [20] L.S. Birks, H. Friedman, Particle size determination from X-ray line broadening, *J. Appl. Phys.* 17 (1946) 687–692.
- [21] J.R. Bolton, K.G. Bircger, W. Tumas, C.A. Tolman, Figure of merit for the technical development and application of advanced oxidation technologies for both electric and solar-derived systems, *Pure Appl. Chem.* 73 (2001) 627–637.
- [22] U.G. Akpan, B.H. Hameed, Parameters affecting the photocatalytic degradation of dyes using TiO₂-based photocatalysts: A review, *J. Hazard. Mater.* 170 (2009) 520–529.
- [23] M.A. Behnajady, H. Eskandarloo, Silver and copper co-impregnated onto TiO₂-P25 nanoparticles and its photocatalytic activity, *Chem. Eng. J.* 228 (2013) 1207–1213.